ResearchGate

See discussions, stats, and author profiles for this publication at: https://www.researchgate.net/publication/353600294

Depiction of the genomic and genetic landscape identifies CCL5 as a protective factor in colorectal neuroendocrine carcinoma

Article *in* British Journal of Cancer · July 2021

DOI: 10.1038/s41416-021-01501-y

CITATION
1

READS
30

17 authors, including:

Dong Chen
Zhejiang University
96 PUBLICATIONS **2,335** CITATIONS
SEE PROFILE

Xuanwen Bao
Zhejiang University
32 PUBLICATIONS **330** CITATIONS
SEE PROFILE

Zhou Tong
East China Normal University
27 PUBLICATIONS **143** CITATIONS
SEE PROFILE

Weijia Fang
Zhejiang University
110 PUBLICATIONS **1,425** CITATIONS
SEE PROFILE

Some of the authors of this publication are also working on these related projects:

Cancer Bioinformatics View project

Bi-specific antibody in colorectal cancer View project

All content following this page was uploaded by Xuanwen Bao on 31 July 2021.

The user has requested enhancement of the downloaded file.

British Journal of Cancer www.nature.com/bjc

ARTICLE

Genetics and Genomics

Depiction of the genomic and genetic landscape identifies CCL5 as a protective factor in colorectal neuroendocrine carcinoma

Dong Chen[1,6], Xuanwen Bao[2,6], Ruyi Zhang[2,6], Yongfeng Ding[2], Min Zhang[3], Benfeng Li[1], Hangyu Zhang[2], Xiaolin Li[4], Zhou Tong[2], Lulu Liu[2], Xiaohu Zhou[5], Saisai Wang[1], Xiaofei Cheng[1], Yi Zheng[2], Jian Ruan[2]✉, Weijia Fang[2]✉ and Peng Zhao[2]✉

© The Author(s), under exclusive licence to Springer Nature Limited 2021

BACKGROUND: Colorectal neuroendocrine carcinomas (CRNECs) are highly aggressive tumours with poor prognosis and low incidence. To date, the genomic landscape and molecular pathway alterations have not been elucidated.
METHODS: Tissue sections and clinical information of CRNEC ($n = 35$) and CR neuroendocrine tumours (CRNETs) ($n = 25$) were collected as an in-house cohort (2010–2020). Comprehensive genomic and expression panels (AmoyDx® Master Panel) were applied to identify the genomic and genetic alterations of CRNEC. Through the depiction of the genomic landscape and transcriptome profile, we compared the difference between CRNEC and CRNET. Reverse transcription-polymerase chain reaction and immunofluorescence staining were performed to confirm the genetic alterations.
RESULTS: High tumour mutation load was observed in CRNEC compared with CRNET. CRNECs showed a "cold" immune landscape and increased endothelial cell activity compared with NETs. Importantly, PAX5 was aberrantly expressed in CRNEC and predicted a poor prognosis of CRNECs. CCL5, a factor that is considered an immunosuppressive factor in several tumour types, was strongly expressed in CRNEC patients with long-term survival and correlated with high $CD8^+$ T cell infiltration.
CONCLUSION: Through the depiction of the genomic landscape and transcriptome profile, we demonstrated alterations in molecular pathways and potential targets for immunotherapy in CRNEC.

British Journal of Cancer; https://doi.org/10.1038/s41416-021-01501-y

INTRODUCTION

Neuroendocrine neoplasms (NENs) were divided into neuroendocrine tumour (NET) low grade, NET intermediate grade, NET high grade and neuroendocrine carcinoma (NEC) based on their molecular differences by the World Health Organisation classification 2019 [1], in which an important change concerns the recognition that well-differentiated NETs may be high grade. Although NEC of the colon and rectum (CRNEC) is a rare NEN type that accounts for 0.1–0.6% of all colorectal malignancies, it is one of the most lethal types of NENs [2, 3]. Due to the rare occurrence of CRNEC, few studies have addressed genomic changes and genetic alterations in CRNEC. Most studies on NEC are based on NEC derived from other locations, such as the lung, pancreas or other organs. Many previous studies have focused on genomic changes in NEC. For instance, Chen et al. demonstrated that *TP53* (65.5%), *APC* (59.5%), *KRAS* (36.9%), *BRAF* (20.2%) and *RB1* (16.7%) were the most common genes harbouring somatic mutations [4]. A total of 88.2% of BRAF mutations were V600E, representing a promising treatment target [4]. Dizdar et al. found high frequencies of the $BRAFV^{600E}$ mutation along with elevated levels of phosphorylated MEK in CRNEC [5]. Nevertheless, CRNEC exhibited poor prognostic properties compared with CRNET, which warrants the exploration of effective therapeutic strategies by analysing both alterations at the genomic and genetic levels.

In this study, we sought to define the genomic and molecular alterations of CRNEC. We collected 26 cases of CRNET and 23 cases of CRNEC in our hospital and evaluated the genomic and genetic alterations by a novel large-scale panel and validated them by reverse transcription-polymerase chain reaction (RT-PCR) and immunofluorescence (IF) staining.

MATERIALS AND METHODS

Sample collection

Informed consent was obtained from each patient. All samples were fully anonymised. NGS analyses were performed according to protocols

[1]Department of Colorectal Surgery, The First Affiliated Hospital Zhejiang, University School of Medicine, Hangzhou, China. [2]Department of Medical Oncology, The First Affiliated Hospital Zhejiang, University School of Medicine, Hangzhou, China. [3]College of Medicine, Zhejiang University, Hangzhou, Zhejiang Province, China. [4]Department of Emergency, The First Affiliated Hospital Zhejiang, University School of Medicine, Hangzhou, Zhejiang Province, China. [5]Department of Hepatobiliary and Pancreatic Surgery, The Second Affiliated Hospital, Zhejiang University School of Medicine, Hangzhou, Zhejiang Province, China. [6]These authors contributed equally: Dong Chen, Xuanwen Bao, Ruyi Zhang. ✉email: software233@zju.edu.cn; weijiafang@zju.edu.cn; zhaop@zju.edu.cn

Received: 6 February 2021 Revised: 20 June 2021 Accepted: 16 July 2021
Published online: 30 July 2021

Table 1. Patient characteristics.

Characteristic	Total No. (%)	NET No. (%)	NEC No. (%)
No. of patients	60	25	35
Median age, years (range)	57.5 (18–90)	60 (31–76)	57 (18–90)
Male sex	33 (55%)	12 (48%)	21 (60%)
DNA sequencing	48 (80%)	23 (92%)	25 (71.4%)
RNA sequencing	38 (63.6%)	21 (84%)	17 (48.6%)
TMB			
<143/Mb	30 (50%)	10 (40%)	20 (57.1%)
143–247/Mb	4 (6.7%)	3 (12%)	1 (2.9%)
>247/Mb	12 (20%)	9 (36%)	3 (8.6%)
Missing	14 (23.3%)	3 (12%)	11 (31.4%)
AJCC			
I	23 (38.3%)	18 (72%)	5 (14.3%)
II	8 (13.3%)	2 (8%)	6 (17.1%)
III	24 (40%)	5 (20%)	19 (54.3%)
IV	5 (8.3%)	0	5 (14.3%)
Ki-67			
<3%	2 (3.3%)	2 (8%)	0
3–20%	23 (38.3%)	23 (92%)	0
>20%	35 (58.3%)	0	35 (100%)
CgA postive	42 (72%)	20 (80%)	22 (62.9%)
Syn postive	55 (91.7%)	25 (100%)	30 (85.7%)
CD56 postive	46 (76.7%)	23 (92%)	23 (65.7%)
CK (pan) postive	40 (66.7%)	22 (88%)	18 (51.4%)
CDX2 postive	6 (10%)	0	6 (17.1%)
CK20 postive	8 (13.3%)	0	8 (22.9%)

reviewed and approved by the Ethics Committee of the First Affiliated Hospital of Zhejiang University. The detailed patient information is given in Table 1. All NET samples were collected from the rectum. All samples were archived and were taken when performing the surgery. Tissues were all from a single time point for each patient. The workflow is shown in Figure S1.

DNA and RNA extraction and library preparation

The DNA and RNA extraction process was described in the previous literature with minor modifications [6, 7]. Total DNA and RNA were extracted from formalin-fixed, paraffin-embedded (FFPE) tumour samples using MagPure FFPE DNA LQ Kit (Cat. # D6323, Magen) and AmoyDx® FFPE RNA Extraction Kit (Cat. # 8.02.24101X036G, AmoyDx), respectively. Quantification of DNA and RNA concentration was performed by Quantus fluorometer and Quantus dsDNA/RNA HS Assay Kit (Cat. # E2670/E3310, Promega). Fragment length was assessed using an Agilent 2100 Bioanalyzer and DNA/RNA HS Kit (Cat. # 5067-1504/5067-1511, Agilent).

DNA was sheared into 200–250 bp fragments using Covaris LE220 (Woburn, MA, USA) and indexed NGS libraries were prepared by end-repairing, A-tailing, adaptor ligation and amplification procedures using NEBNext® Ultra™ II DNA Prep Kit (Cat. #E7645, NEB). RNA was fragmented at 95 °C for 0–15 min according to the DV200 value estimated by Agilent 2100 Bioanalyzer System. RNA fragments then undergo reverse transcription, complementary DNA synthesis and strand-specific library preparation using NEBNext® Ultra™ II Directional RNA Library Prep Kit for Illumina® (Cat. #E7760L, NEB).

Hybrid capture and sequencing

DNA and RNA libraries were captured separately by AmoyDx® Master Panel, which contains 559 genes for DNA mutation (single-nucleotide variation (SNV), insertion/deletion (Indel), Fusion, copy number variation, microsatellite instability and tumour mutation burden (TMB)) detection and 1813 genes for RNA expression and fusion detection. Captured products were amplified and quantified by a Quantus fluorometer. Library size was assessed using Agilent 2100 Bioanalyzer. After pooling, libraries were then sequenced on Illumina NovaSeq 6000 instrument (Illumina) with 2×150 bp pair-end reads. Sequencing data were analysed and annotated with an in-house developed pipeline. A set of experimental and data quality control parameters were set up.

Mutation calling and filtering

The average coverage depth was 813.9X for tumours. Sequencing data were first cleaned to remove sequencing adaptors and low-quality reads (quality <15) or poly-N with Trimmomatic and mapped to the human reference genome, version 19 (hg19) using the Burrows-Wheeler Aligner. PCR duplicates were marked and removed using Mark Duplicates from the Genome Analysis Toolkit (GATK). Base Quality Score Recalibration was performed using GATK's BaseRecalibrator and ApplyBQSR. After correction, a bam file was acquired. The Indels and single-nucleotide polymorphisms were compared by Mutect2 and FilterMutectCalls of GATK to obtain the final vcf file. Analysis of variance was used to annotate the vcf files. SNVs and Indels called were further filtered using the following criteria: (i) minimum ≥5 variant supporting reads and ≥5% variant allele frequency supporting the variant, (ii) filtered if present in >2% population frequency in the 1000g or ExAC or GnomAD database, (iii) filtered if variants not located in CDS region, (iv) filtered if variants were not annotated as (likely/predicted) oncogenic in the OncoKB database. These filtered variants were functional and were used for subsequent data analysis. Detailed information is shown in Table S1.

Differential expression and KEGG pathway analysis

The differential genes between NET and NEC was analysed with RNA count data using R package DESeq2 [8], and the online g:Profiler analysis tool (https://biit.cs.ut.ee/gprofiler/gost) was used for enrichment analysis. In order to explore the differential pathways between NET and NEC, R package GSVA (gene set variation analysis) [9] was used to calculate the KEGG pathway enrichment score for each sample, and hierarchical clustering was then performed to get the dendrogram of KEGG pathways with average distance. Student's *t* test was performed for statistical significance between NET and NEC GSVA scores.

RT-PCR

Differential expression of six candidate genes between NET and NEC were validated by real-time PCR using the SLAN-96S detection system (Hongshi, Shanghai). The primer sequencing information was in Table S2. The amplifications were done using Real-time PCR Master Mix (Amoy Diagnostics). The thermal cycling conditions were composed of 50 °C for 2 min, followed by an initial denaturation step at 95 °C for 5 min, 40 cycles at 95 °C for 10 s, 60 °C for 25 s and 72 °C for 10 s. The experiments were carried out in duplicate for each data point. The relative quantification in gene expression was determined using the $2^{-\Delta\Delta Ct}$ method. Using this method, we obtained the fold changes in gene expression normalised to an internal control gene.

Survival analysis

Python package lifelines (version 0.24.1) was used to perform survival analysis, including Kaplan–Meier (KM) curves and Cox regression analysis. The log-rank test was performed for KM curves statistical significance testing.

Immunofluorescence

The tissue sections were immersed twice in xylene for 15 min and anhydrous ethanol for 5 min. Then, the tissue sections were successively soaked in 85% alcohol for 5 min, 75% alcohol for 5 min and finally rinsed with distilled water. After the paraffin sections were deparaffinized with water, they were placed in a pressure cooker filled with citric acid (pH 6.0; Servicebio, G1202) antigen retrieval solution for antigen retrieval. When the pressure cooker gushed out the gas evenly for 3 min, the heating was stopped. After natural cooling to room temperature, the slides were placed in phosphate-buffered saline (PBS; Servicebio, G0002) and washed by shaking on a decolourising shaker (Servicebio, TSY-B) three times (5 min each). The sections were shaken dry and circled with a histochemical marker (Gene Tech, GT1001) to prevent the antibodies from flowing away.

Monoclonal antibodies (mAbs) were used as follows: anti-CD8-mAb (1:200; Servicebio, GB13068-2), anti-CCL5-mAb (1:200; bioss, bs-20765R),

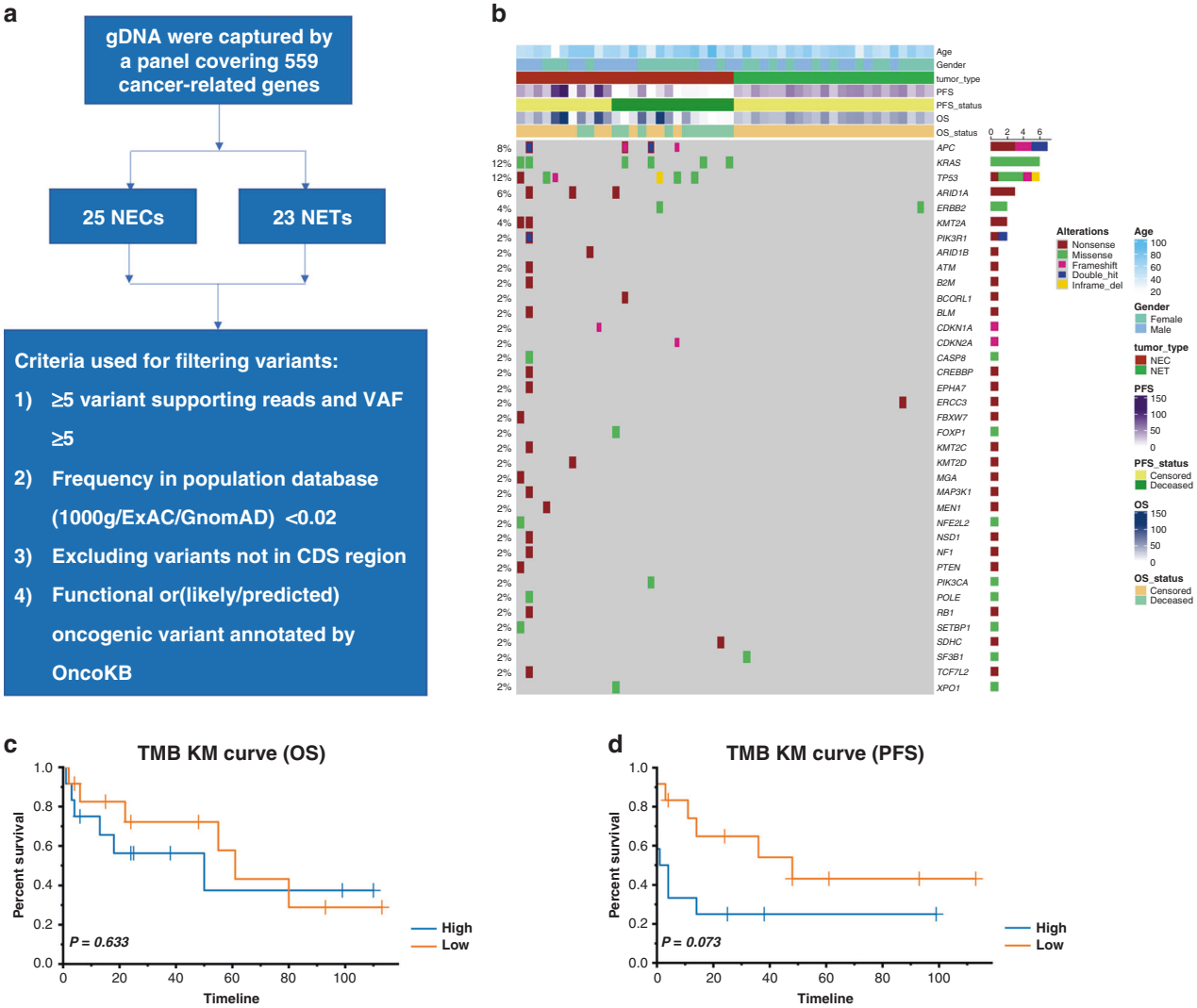

Fig. 1 The genomic landscape of CRNEC and CRNET. a Workflow depiction of the genomic landscape. **b** Oncoplot of genomic alterations in CRNEC and CRNET. **c** The association between OS and TMB in CRNEC patients. **d** The association between PFS and TMB in CRNEC patients. Twenty-three CRNET samples and 25 CRNEC samples were applied in the DNA-sequencing analysis.

anti-PAX5-mAb (1:100; zsbio, ZA-0566), Cy3-conjugated goat anti-rabbit IgG (1:300; Servicebio, GB21303) and 488-conjugated goat anti-rabbit IgG (1:400; Servicebio, GB25303).

The IF double staining was carried out for CCL5 and CD8 or PAX5 and CD8 according to standard staining procedures. Before primary antibody incubation, 5% bovine serum albumin was added to the circle for blocking for 30 min. After the blocking solution was gently shaken off, the sections were put in a wet chamber and incubated with a primary antibody at 4 °C overnight. The slides were then washed with PBS buffer three times (5 min each). Later, the slides were incubated with a secondary antibody in the dark at room temperature for 50 min, followed by washing in PBS buffer. The autofluorescence quencher (Servicebio) was then added into the ring for 5 min and then washed with running water for 20 min. After the slices were slightly dried, 4,6-diamidino-2-phenylindole (Servicebio, G1012) was added into the circles and incubated at room temperature in the dark for 10 min. After the sections were washed with PBS buffer and dried, they were mounted with anti-fluorescence quenching mounting tablets (Servicebio, G1401). The slides were digitised using a fluorescence microscope (NIKON DS-U3) at ×20 magnification.

RESULTS

Depiction of the genomic landscape of CRNET and CRNEC

We performed large-panel genomic analysis on CRNET and CRNEC tissue samples (Fig. 1a, b). *KRAS* was the most frequently mutated gene in the cohort. *KRAS*, *TP53*, *APC*, *ARID1A* and *ERBB2* were the top 5 most mutated genes in our CRNEC and CRNET cohort. The KM plot indicated that the TMB value was not significantly associated with the overall survival (OS) or progression-free survival (PFS) of CRNEC (Fig. 1c, d).

Differences in transcriptome profiles and molecular pathways between CRNET and CRNEC

We then compared the transcriptome differences between CRNEC and CRNET tissues. A volcano plot indicated that 187 genes were differentially expressed (threshold: fold change >2 and adjusted P value < 0.05) (Fig. 2a). KEGG analysis indicated that cancer-related pathways such as Wnt signalling, PI3K-Akt signalling, cell cycle and Ras signalling were enriched. GO analysis revealed that signalling receptor binding, receptor regulator activities, signalling receptor activator activities and other biological processes were enriched (Fig. 2b). Using the GSVA method, we performed a single-sample gene set enrichment analysis, and the results indicated that glycosaminoglycan (GAG) degradation, pentose and glucuronate interconversions, cysteine and methionine metabolism, GAG biosynthesis chondroitin sulfate (CS) and GAG biosynthesis heparan sulfate (HS) were significantly upregulated in NECs compared with NETs (Fig. 2c).

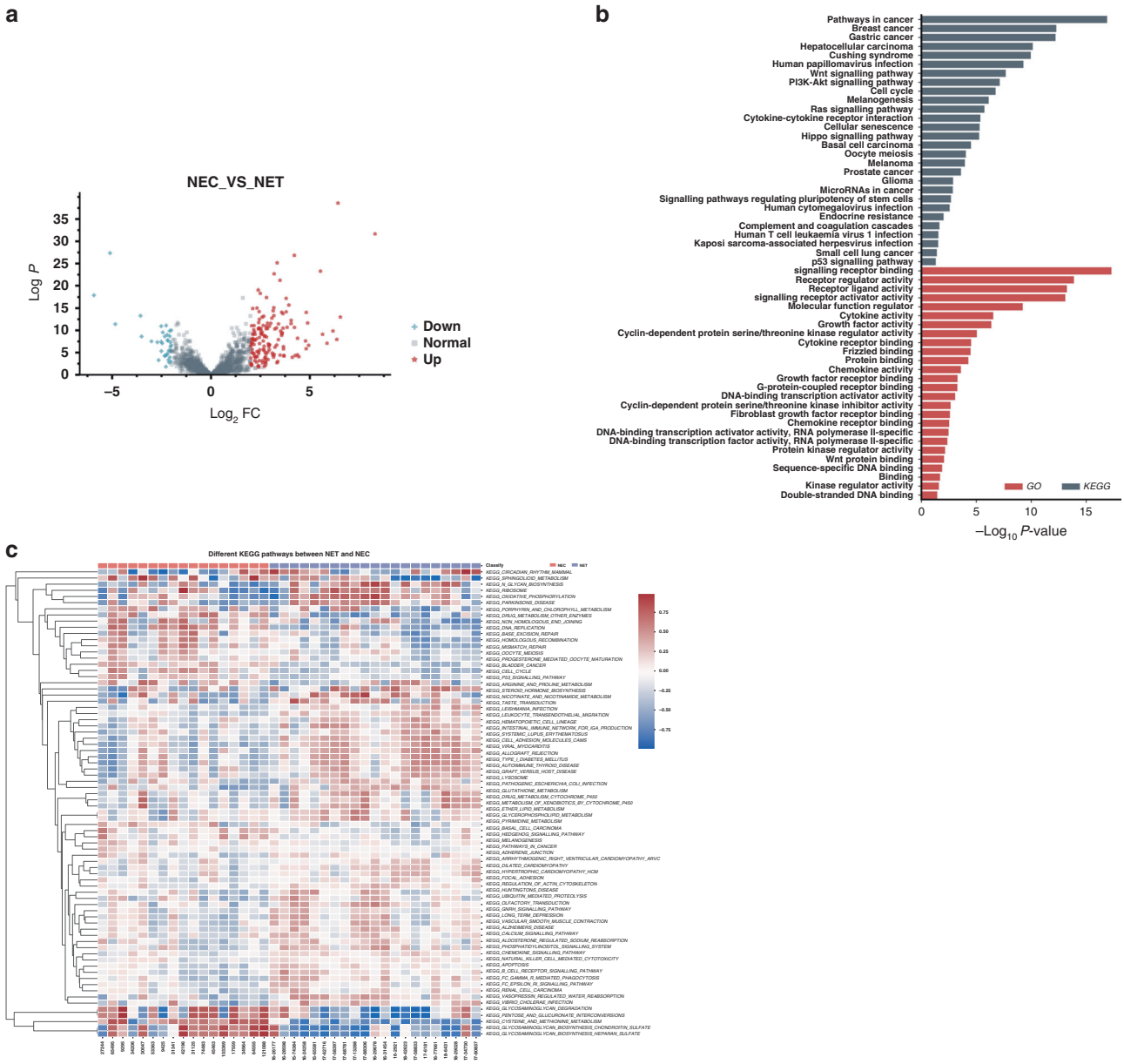

Fig. 2 Comparison of transcriptome profiles between NEC and NET. a The volcano plot indicates the DEGs between CRNEC and CRNET. **b** GO and KEGG pathway analysis based on the DEGs between CRNEC and CRNET. **c** Heatmap showing the GSVA score for KEGG pathways of each sample. Twenty-one CRNET samples and 17 CRNEC samples were applied in the RNA-sequencing analysis.

Immune landscape-related prognostic factors in CRNEC

The NEC samples were separated into long- and short-term survival (the cut-offs for the samples was a median value: short-term survival: <13 months; long-term survival: ≥13 months). Differentially expressed gene (DEG) analysis was performed between these two groups. The significant DEGs from the comparison between NEC and long- and short-term survival were identified, followed by overlapping with the DEGs from the comparison between NET and NEC. The results indicated that *PAX5*, *H3C10*, *MKI67*, *MCM7*, *XRCC2*, *CDK4*, *SMARCA4*, *CDKN2A*, *PMAIP1*, *CCL5* and *GSTT1* were the most significant DEGs and the expression of these identified genes were shown in the total cohort (Fig. 3a). MCPCOUNTER was performed to explore the immune microenvironment, and the results indicated that $CD8^+$ T cells, B cells, myeloid dendritic cells and macrophages/monocytes were enriched in NETs compared with NECs. These features are indicative of a more active immune microenvironment in NET tissues (Fig. 3a). In contrast, the signature of endothelial cells was highly expressed in NEC tissues, indicating a microenvironment of tumour vessel hyperplasia in NEC tissues.

In particular, *CCL5* was upregulated in NEC samples compared with NET samples. We then focused on NEC and found that *CCL5* was upregulated, whereas *CDNK2A*, *PAX5*, *PMAIP1*, *H3C10*, *MKI67*, *CDK4*, *SMARCA4*, *MCM7* and *XRCC2* were downregulated in the long-term OS group (Fig. 3b). Univariate Cox analysis revealed that *PAX5*, *CDK4*, *CDKN2A*, *MKI67* and *H3C10* were associated with poor survival of patients with NEC, whereas *CCL5* indicated poor prognosis in NEC patients (Fig. 3c and Table S3, respectively). The OS of CRNEC was stratified by *PAX5*, *CDK4*, *CDKN2A*, *MKI67*, *H3C10* and *CCL5*, as shown by a KM plot (Fig. 3d–l). Furthermore, the expression level of *PAX5*, *CDK4*, *CDKN2A*, *MKI67*, *H3C10* and *CCL5* between NEC and NET was validated by RT-PCR (Fig. 4a–f).

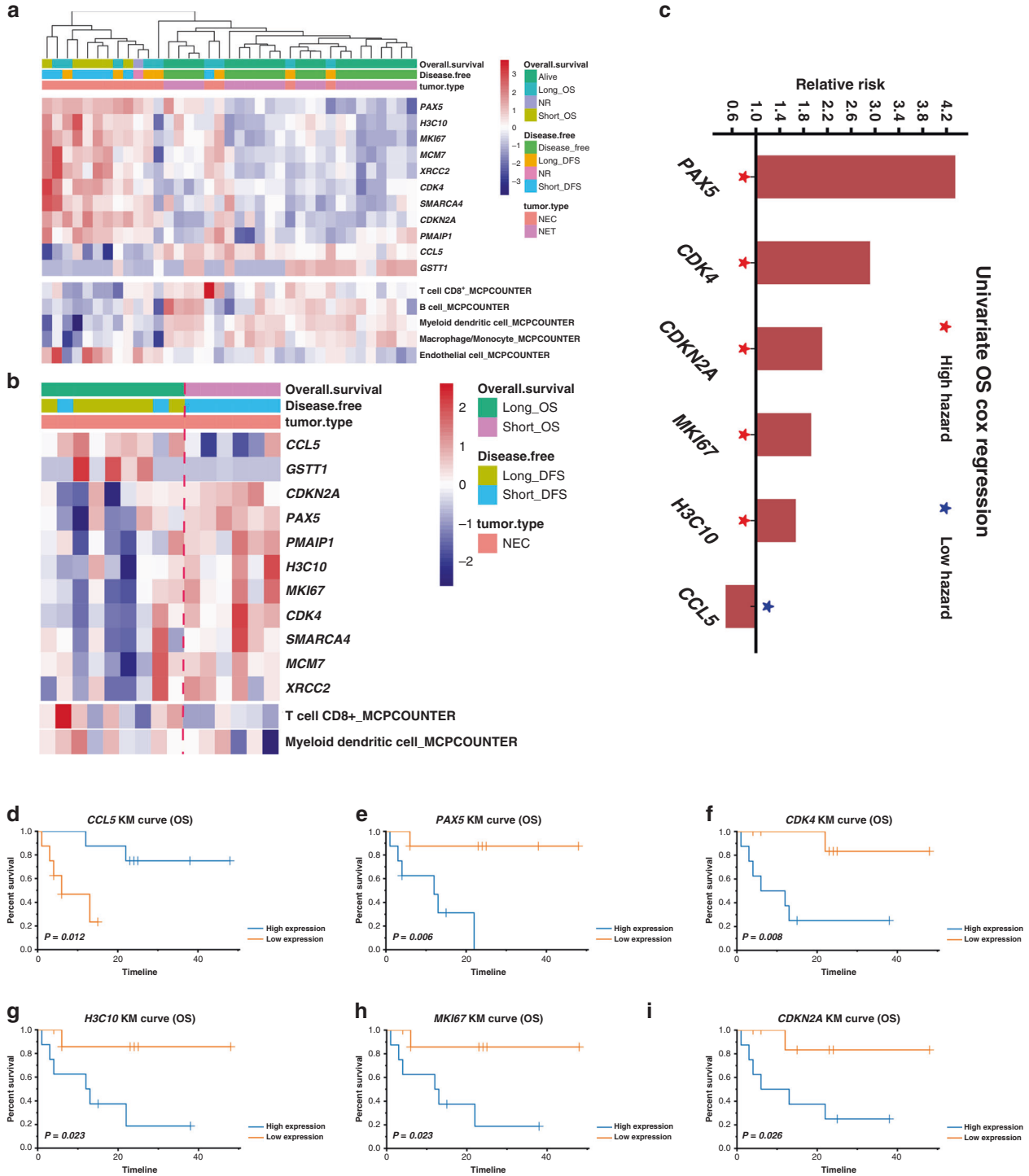

Fig. 3 Genetic alterations in CRNEC and potential targets for immunotherapy. a Heatmap showing the most significant DEGs and microenvironmental components between CRNEC and CRNET. **b** Heatmap showing the most significant DEGs and microenvironmental components between long-OS and short-OS CRNEC. **c** The hazard ratio for the genes that were significantly associated with OS in CRNEC. **d–i** The OS of CRNEC is stratified by *CCL5*, *PAX5*, *CDK4*, *H3C10*, *MKI67* and *CDKN2A*. *X*-axis of Kaplan–Meier plot: months. NR not reached the endpoint. Only the patients who reached the endpoint (deceased or relapsed) were included in the analysis based on short- and long-term survival. Twenty-one CRNET samples and 17 CRNEC samples were applied in the RNA-sequencing analysis.

Contradictory results regarding the function of *CCL5* in the tumour immune microenvironment (TME) and the prognostic value of *CCL5* were observed in different tumour types. In most studies, *CCL5* was a key factor in immune escape and thus a prognostic factor that shortens the OS of patients [10–13]. Nevertheless, in our study on CRNEC, we confirmed that *CCL5* was highly expressed in patients with long-term survival and high $CD8^+$ T cell infiltration by expression profiling. To confirm the previous results, we performed double IF staining on CD8 and *CCL5* in CRNEC and CRNET tissues. The results indicated that tissues with high $CD8^+$ T cell infiltration also had more CCL5-positive cells. In addition, CRNET had more CCL5-positive cells and

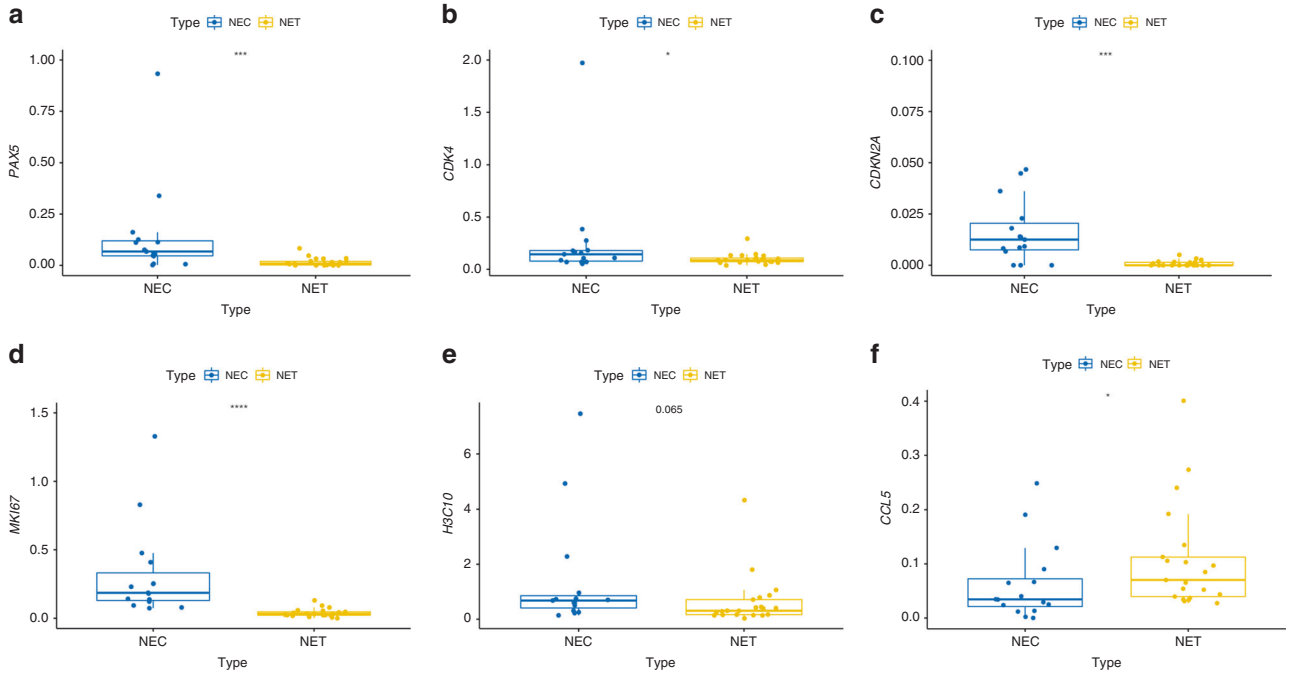

Fig. 4 RT-PCR for targeted genes. a Relative expression of PAX5 between NET and NEC. **b** Relative expression of CDK4 between NET and NEC. **c** Relative expression of CDKN2A between NET and NEC. **d** Relative expression of MKI67 between NET and NEC. **e** Relative expression of H3C10 between NET and NEC. **f** Relative expression of CCL5 between NET and NEC. NEC sample number used: 14. NET sample number used: 14.

$CD8^+$ T cell infiltration than CRNEC (Fig. 5a). In contrast, tissues with more PAX5-positive cells was associated with low $CD8^+$ T cell infiltration. PAX5 was expressed in CRNEC tissues but rarely expressed in CRNET tissues (Fig. 5b). Multivariate Cox regression for the expression of *CCL5*, *PAX5* and other clinicopathological characteristics also confirmed the results above (Tables S4–5, respectively).

DISCUSSION

In this study, we performed a comprehensive analysis of CRNEC based on genomic and transcriptomic landscapes. A similar mutation pattern can be identified in CRNEC and colorectal adenocarcinoma. *TP53*, *ARID1A* and *APC*, which were frequently mutated in colorectal adenocarcinoma, were also found to be commonly altered in CRNEC. One study demonstrated that CRNEC shared more similarities with colorectal adenocarcinoma compared to its NET counterparts regarding genomic alterations, which was consistent with our findings. NECs exhibited a "cold" immune landscape and higher endothelial cell activity than NETs, which may induce immune escape in NEC tissues. PAX5 may act as an immunosuppressive factor associated with poor prognosis in CRNEC. CCL5 is a chemokine that is involved in the immunoregulatory process and is an indicator of poor prognosis in several tumour types. CCL5 was strongly expressed in NEC patients with long-term survival. With the conformation of IF staining, we demonstrated that CCL5 may play a unique role in regulating the NEC immune microenvironment and improve the prognosis of NEC patients.

A higher tumour burden load was observed in NEC compared with NET. Given the limited sample size of NEC tissues, no significant association between TMB and survival was found. Nevertheless, the high tumour burden load in NEC may provide a potential better response to ICI-based immunotherapy and the opportunity for the application of neoantigen-based immunotherapy.

Significant differences in transcriptome expression levels and pathway activation were found between CRNEC and CRNET tissues. In particular, GAG-related pathways were significantly activated in NEC samples. CS and HS are the two most common forms of sulfated GAGs, which play crucial roles in both extracellular and cellular locations [14]. They have controversial roles that promote or inhibit tumour progression depending on the stage or type of cancer [15–17]. In CRNEC, CS and HS activities were significantly increased compared with those of CRNET, which is consistent with one previous study on gastroenteric, pancreatic and pulmonary neuroendocrine tumours [14].

Alvarez et al. revealed the presence of tumour master regulators of gastroenteropancreatic NENs (GEP-NENs) in vitro, and their targeting in vitro by some special inhibitors led to a tumour checkpoint collapse. GEP-NEN molecular subtypes and master regulators for metastatic progression of GEP-NETs (primary tumours vs hepatic metastases) were identified by the transcriptome data. Several key factors, including IL2RB1, IL10, CIITA, CD45, CD53, CD86 and RUNX3, were found to play crucial roles in reprogramming to a more malignant phenotype and help immune escape. Thus, the tumour microenvironment of GEP-NENs is considered to be immunosuppressive and suitable for metastasis. To further explore the detailed mechanism underlying the immunosuppressive tumour microenvironment of NENs, we performed DEGs between CRNEC and CRNET. *PAX5*, *H3C10*, *MKI67*, *XRCC2* and *CDK4* were upregulated, whereas *CCL5* and *GSTT1* were downregulated in CRNEC. The upregulation of *MKI67* and *CDK4*, which are proliferation markers and key components of the cell cycle, respectively, indicated that NECs exhibit a more progressive phenotype than CRNETs. *XRCC2*, a crucial gene involved in mismatch repair, was also upregulated in CRNEC. Taken together, dysregulation of the cell cycle, DNA repair and proliferation-related genes in CRNEC contribute to tumour progression and higher staging of CRNEC. In addition, the signature for endothelial cells was upregulated in CRNEC, suggesting that CRNEC exhibited more aggressive properties than CRNET.

Surprisingly, we found that CCL5 expression was higher in CRNETs than in CRNECs. In contrast, PAX5 was aberrantly expressed in NECs compared with NETs. Furthermore, low CCL5

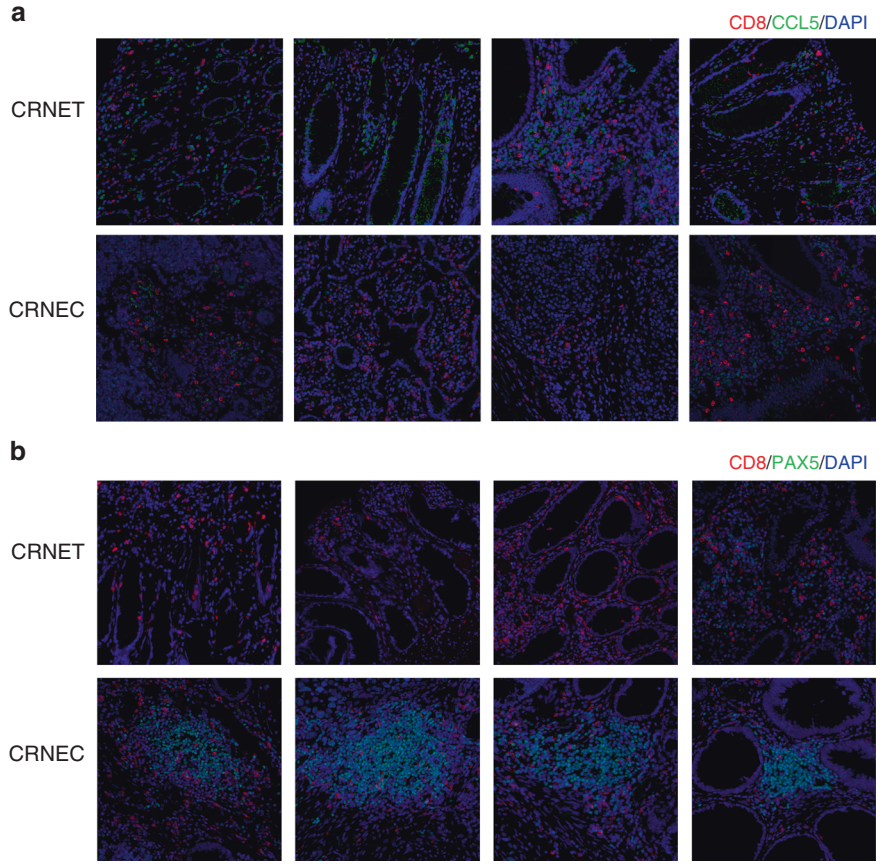

Fig. 5 Immunofluorescence double staining. a *CCL5* and *CD8*. **b** *PAX5* and *CD8*. NEC sample number used: 10. NET sample number used: 10.

expression and high PAX5 expression were observed in CRNEC patients with poor survival outcomes and low $CD8^+$ T cell abundance. CCL5 and PAX5 are both crucial factors involved in regulating the tumour immune microenvironment. PAX5 is a member of the PAX family and plays an important role in B cell development [18] and acts as an oncogene in various tumour types [19–21]. PAX5 expression is limited in human solid tissues, whereas aberrant expression of PAX5 was observed in several solid tumours, which made it a potential neoantigen [21]. One study reported an immunogenic HLA-A2-restricted epitope sequence (TLPGYPPHV) in human PAX5, a potent stimulator of specific anti-PAX5 T cell-mediated responses [21]. We found that PAX5 was highly expressed in CRNEC and associated with poor survival of CRNEC patients, making it a promising target for neoantigen-based immunotherapy in CRNEC.

The CCL5/CCR5 axis plays crucial roles in cancer progression, including extracellular matrix remodelling [22], tumour growth and metastasis [23], cancer stem cell proliferation [24], DNA damage repair [25], angiogenesis [26], autocrine/paracrine signalling [27] and metabolic reprogramming [28]. Aberrant CCL5 and CCR5 expression can be caused by the recruitment and accumulation of CCR5-positive cells into the TME or the education of normal cells, which has been reported in various tumour types [29]. For instance, CCL5 is overexpressed in CRC cells at the primary location and liver and lung metastases [30]. CCL5 expression levels were also increased in blood samples from CRC patients compared to blood samples from healthy donors [31]. Furthermore, the CCL5/CCR5 axis reshapes the immunosuppressive TME by increasing the infiltration of T-regulatory cells and promoting the polarisation of monocytes into M2-phenotype TAMs [32]. Different approaches have been used to block the CCL5/CCR5 axis, such as inhibition of CCR5 with antagonists, inhibition of CCL5 expression with neutralising antibodies or gene silencing [10]. However, CCL5 can also promote antitumour immunity by recruiting antitumour T cells into the TME, thus enhancing the response to immunotherapy in several tumour types [33–37]. One recent study showed that $CD8^+$ T cells were attracted to the tumour epithelium through CCL5 overexpression in DNA mismatch repair-deficient (dMMR) CRC [38]. This process was dependent on endogenous activation of the cGAS/STING and interferon signalling pathways by damaged DNA in dMMR-CRCs [38]. In our CRNEC cohort, we found that CCL5 was correlated with high $CD8^+$ T cell abundance and was associated with a better prognosis in CRNEC patients. As discussed above, CRNEC shared similarities with colorectal adenocarcinoma regarding genomic alterations. Here, our results also implied the potential of TME similarities between colorectal adenocarcinoma and CRNEC.

There are still some limitations to our study. Although we recruited 60 cases of tumour tissues, we were not able to perform sequencing analysis in all of the samples due to the quality control. Only 48 cases were analysed on the DNA level and 38 cases were analysed on RNA level, respectively. In addition, the lack of external validation may have reduced the reliability of our conclusion. The long-term timeframe for the comparison of samples from different periods should also be noticed.

In summary, we compared the genomic and genetic differences between CRNET and CRNEC. Importantly, PAX5 and CCL5, two key components in reshaping the TME, were associated with $CD8^+$ T cell abundance and prognosis in CRNEC patients. PAX5 was associated with poor survival and low $CD8^+$ T cell infiltration in

CRNEC. Unlike various cancer types, CCL5 exhibited a positive correlation with $CD8^+$ T cell activity and predicted a better prognosis in CRNEC. The results of this study may help to characterise CRNEC and identify patients that may respond to immunotherapy.

DATA AVAILABILITY

All presented data in this study are available from the corresponding author upon reasonable request.

REFERENCES

1. Nagtegaal ID, Odze RD, Klimstra D, Paradis V, Rugge M, Schirmacher P, et al. The 2019 WHO classification of tumours of the digestive system. Histopathology 2020;76:182–8.
2. Bertani E, Ravizza D, Milione M, Massironi S, Grana CM, Zerini D, et al. Neuroendocrine neoplasms of rectum: a management update. Cancer Treat. Rev. 2018;66:45–55.
3. Dasari A, Shen C, Halperin D, Zhao B, Zhou S, Xu Y, et al. Trends in the incidence, prevalence, and survival outcomes in patients with neuroendocrine tumors in the United States. JAMA Oncol. 2017;3:1335–42.
4. Chen L, Liu M, Zhang Y, Guo Y, Chen M-H, Chen J. Genetic characteristics of colorectal neuroendocrine carcinoma: more similar to colorectal adenocarcinoma. Clin Colorectal Cancer. 2021;20:177–85.e13.
5. Dizdar L, Werner TA, Drusenheimer JC, Möhlendick B, Raba K, Boeck I, et al. BRAFV600E mutation: a promising target in colorectal neuroendocrine carcinoma. Int J Cancer. 2019;144:1379–90.
6. Liu L, Zhang R, Deng J, Dai X, Zhu X, Fu Q, et al. Construction of TME and identification of crosstalk between malignant cells and macrophages by SPP1 in hepatocellular carcinoma. Cancer Immunol Immunother. 2021:1–16. https://doi.org/10.1007/s00262-021-02967-8. Online ahead of print
7. Bao X, Zhang H, Wu W, Cheng S, Dai X, Zhu X, et al. Analysis of the molecular nature associated with microsatellite status in colon cancer identifies clinical implications for immunotherapy. J Immunother Cancer. 2020;8:e001437.
8. Love MI, Huber W, Anders S. Moderated estimation of fold change and dispersion for RNA-seq data with DESeq2. Genome Biol. 2014;15:550.
9. Hänzelmann S, Castelo R, Guinney J. GSVA: gene set variation analysis for microarray and RNA-seq data. BMC Bioinform. 2013;14:7.
10. Aldinucci D, Borghese C, Casagrande N. The CCL5/CCR5 axis in cancer progression. Cancers 2020;12:1765.
11. Walens A, DiMarco AV, Lupo R, Kroger BR, Damrauer JS, Alvarez JV. CCL5 promotes breast cancer recurrence through macrophage recruitment in residual tumors. Elife 2019;8:e43653.
12. Huang R, Wang S, Wang N, Zheng Y, Zhou J, Yang B, et al. CCL5 derived from tumor-associated macrophages promotes prostate cancer stem cells and metastasis via activating β-catenin/STAT3 signaling. Cell Death Dis. 2020;11:1–20.
13. Zazo S, González-Alonso P, Martin-Aparicio E, Chamizo C, Luque M, Sanz-Alvarez M, et al. Autocrine CCL5 effect mediates trastuzumab resistance by ERK pathway activation in HER2-positive breast cancer. Mol Cancer Ther. 2020;19:1696–707.
14. García-Suárez O, García B, Fernández-Vega I, Astudillo A, Quirós LM. Neuroendocrine tumors show altered expression of chondroitin sulfate, glypican 1, glypican 5, and syndecan 2 depending on their differentiation grade. Front Oncol. 2014;4:15.
15. Afratis N, Gialeli C, Nikitovic D, Tsegenidis T, Karousou E, Theocharis AD, et al. Glycosaminoglycans: key players in cancer cell biology and treatment. FEBS J. 2012;279:1177–97.
16. Lindahl U, Kjellén L. Pathophysiology of heparan sulphate: many diseases, few drugs. J Intern Med. 2013;273:555–71.
17. Iozzo RV, Sanderson RD. Proteoglycans in cancer biology, tumour microenvironment and angiogenesis. J Cell Mol Med. 2011;15:1013–31.
18. Busslinger M. Transcriptional control of early B cell development. Annu Rev Immunol. 2004;22:55–79.
19. Souabni A, Jochum W, Busslinger M. Oncogenic role of Pax5 in the T-lymphoid lineage upon ectopic expression from the immunoglobulin heavy-chain locus. Blood 2007;109:281–9.
20. Robichaud GA, Nardini M, Laflamme M, Cuperlovic-Culf M, Ouellette RJ. Human Pax-5 C-terminal isoforms possess distinct transactivation properties and are differentially modulated in normal and malignant B cells. J Biol Chem. 2004;279:49956–63.
21. Yan M, Himoudi N, Pule M, Sebire N, Poon E, Blair A, et al. Development of cellular immune responses against PAX5, a novel target for cancer immunotherapy. Cancer Res. 2008;68:8058–65.
22. Do HTT, Lee CH, Cho J. Chemokines and their receptors: multifaceted roles in cancer progression and potential value as cancer prognostic markers. Cancers. 2020;12:287.
23. Aldinucci D, Borghese C, Casagrande N. Formation of the immunosuppressive microenvironment of classic Hodgkin lymphoma and therapeutic approaches to counter it. Int J Mol Sci. 2019;20:2416.
24. Chang L-Y, Lin Y-C, Mahalingam J, Huang C-T, Chen T-W, Kang C-W, et al. Tumor-derived chemokine CCL5 enhances TGF-β–mediated killing of CD8+ T cells in colon cancer by T-regulatory cells. Cancer Res. 2012;72:1092–102.
25. Jiao X, Velasco-Velázquez MA, Wang M, Li Z, Rui H, Peck AR, et al. CCR5 governs DNA damage repair and breast cancer stem cell expansion. Cancer Res. 2018;78:1657–71.
26. Wang S-W, Liu S-C, Sun H-L, Huang T-Y, Chan C-H, Yang C-Y, et al. CCL5/CCR5 axis induces vascular endothelial growth factor-mediated tumor angiogenesis in human osteosarcoma microenvironment. Carcinogenesis 2015;36:104–14.
27. Ban Y, Mai J, Li X, Mitchell-Flack M, Zhang T, Zhang L, et al. Targeting autocrine CCL5–CCR5 axis reprograms immunosuppressive myeloid cells and reinvigorates antitumor immunity. Cancer Res. 2017;77:2857–68.
28. Yang X, Hou J, Han Z, Wang Y, Hao C, Wei L, et al. One cell, multiple roles: contribution of mesenchymal stem cells to tumor development in tumor microenvironment. Cell Biosci. 2013;3:5.
29. Casagrande N, Borghese C, Visser L, Mongiat M, Colombatti A, Aldinucci D. CCR5 antagonism by maraviroc inhibits Hodgkin lymphoma microenvironment interactions and xenograft growth. Haematologica 2019;104:564–75.
30. Cambien B, Richard-Fiardo P, Karimdjee BF, Martini V, Ferrua B, Pitard B, et al. CCL5 neutralization restricts cancer growth and potentiates the targeting of PDGFRβ in colorectal carcinoma. PLoS ONE. 2011;6:e28842.
31. Üçüncü M, Serilmez M, Sarı M, Bademler S, Karabulut S. The diagnostic significance of PDGF, EphA7, CCR5, and CCL5 levels in colorectal cancer. Biomolecules 2019;9:464.
32. Halama N, Zoernig I, Berthel A, Kahlert C, Klupp F, Suarez-Carmona M, et al. Tumoral immune cell exploitation in colorectal cancer metastases can be targeted effectively by anti-CCR5 therapy in cancer patients. Cancer Cell. 2016;29:587–601.
33. Dangaj D, Bruand M, Grimm AJ, Ronet C, Barras D, Duttagupta PA, et al. Cooperation between constitutive and inducible chemokines enables T cell engraftment and immune attack in solid tumors. Cancer Cell. 2019;35:885–900. e10
34. de Galarreta MR, Bresnahan E, Molina-Sánchez P, Lindblad KE, Maier B, Sia D, et al. β-Catenin activation promotes immune escape and resistance to anti–PD-1 therapy in hepatocellular carcinoma. Cancer Discov. 2019;9:1124–41.
35. Huffman AP, Lin JH, Kim SI, Byrne KT, Vonderheide RH. CCL5 mediates CD40-driven CD4+ T cell tumor infiltration and immunity. JCI Insight. 2020;5:e137263.
36. Böttcher JP, Bonavita E, Chakravarty P, Blees H, Cabeza-Cabrerizo M, Sammicheli S, et al. NK cells stimulate recruitment of cDC1 into the tumor microenvironment promoting cancer immune control. Cell 2018;172:1022–37.e14.
37. Seo W, Shimizu K, Kojo S, Okeke A, Kohwi-Shigematsu T, Fujii S-I, et al. Runx-mediated regulation of CCL5 via antagonizing two enhancers influences immune cell function and anti-tumor immunity. Nat Commun. 2020;11:1–16.
38. Mowat C, Mosley SR, Namdar A, Schiller D, Baker K. Anti-tumor immunity in mismatch repair-deficient colorectal cancers requires type I IFN–driven CCL5 and CXCL10. J Exp Med. 2021;218:e20210108.

AUTHOR CONTRIBUTIONS

DC: investigation, methodology, writing original draft and writing—review and editing. XB: conceptualisation, methodology, data curation, formal analysis, methodology, visualisation, project administration and writing the original draft. RZ: data curation, formal analysis and writing—review and editing. HZ: data curation, formal analysis and writing—review and editing. ZT: data curation, visualisation and writing—review and editing. LL: data curation, validation and writing—review and editing. YZ: data curation, software and writing—review and editing. MZ: data curation, validation and writing—review and editing. XL: validation and writing—review and editing. SW: validation and writing—review and editing. BL: data curation, validation and writing—review and editing. XC: data curation, validation and writing—review and editing. XC: data curation, validation and writing—review and editing. RJ: formal analysis, visualisation, methodology and writing—review and editing. WF: conceptualisation, supervision, funding acquisition and writing—review and editing. PZ: investigation, visualisation, supervision and writing—review and editing.

FUNDING INFORMATION

This study was supported by grants (nos. 81874143, 31971192) from the National Nature Science Foundation of China and grants (LY21H030005, LQ19H160025, LY19H160040) from the Natural Science Foundation of Zhejiang Province.

ETHICS APPROVAL AND CONSENT TO PARTICIPATE

The studies involving human participants were reviewed and approved by the ethics committee of The First Affiliated Hospital, College of Medicine, Zhejiang University. All patients/participants provided informed consent.

CONSENT FOR PUBLICATION

All authors reviewed and approved the manuscript.

COMPETING INTERESTS

The authors declare no competing interests.

ADDITIONAL INFORMATION

Supplementary information The online version contains supplementary material available at https://doi.org/10.1038/s41416-021-01501-y.

Correspondence and requests for materials should be addressed to J.R., W.F. or P.Z.

Reprints and permission information is available at http://www.nature.com/reprints

Publisher's note Springer Nature remains neutral with regard to jurisdictional claims in published maps and institutional affiliations.

View publication stats